Equi-biaxial tension tests on magneto-rheological elastomers

# Equi-biaxial tension tests on magneto-rheological elastomers

**Gerlind Schubert and Philip Harrison**

School of Engineering, University of Glasgow, University Avenue, Glasgow G12 8QQ, UK

E-mail: Philip.Harrison@glasgow.ac.uk

CrossMark

## Abstract

A bespoke test rig has been designed to facilitate testing of magneto-rheological (MR) elastomers (MREs) under equi-biaxial tension using a standard universal test machine. Tests were performed up to 10% strain on both isotropic and anisotropic MREs with and without the application of an external magnetic field. Assumptions regarding the material's response were used to analyse stress–strain results in the two stretching directions. The assumptions have been verified previously by uniaxial tension tests and by simulations of the magnetic flux distribution performed using a commercial multi-physics finite element software. The MR effect, which is defined as the increase in tangent modulus at a given strain, has been studied versus engineering strain. The latter was measured optically in the experiments using a digital image correlation system. Relative MR effects up to 74% were found when the particle alignment of anisotropic MREs was oriented parallel to an applied magnetic induction of just 67.5 mT.

(Some figures may appear in colour only in the online journal)

## 1. Introduction

Magneto-rheological elastomers (MREs) are smart materials which can alter some of their properties reversibly and almost instantaneously by the application of external magnetic fields. This behaviour is caused by the interaction of micron-sized magnetic particles dispersed in an elastomeric material. In MREs the magnetic particles are locked in position in the final product. Isotropic and anisotropic materials can be prepared, the latter by exposing the MRE mixture to a magnetic field while curing; this forces the magnetic particles to align in chains, which results in a strong mechanical and magnetic anisotropy [1]. The dynamic small strain behaviour of MREs is well explored [1–3]; different types of matrix materials and magnetic particles have been studied. Recently, the magnetostriction [4], and the magnetic properties of MREs [5] have also been investigated. Nevertheless, there is still a distinct

lack of knowledge concerning the constitutive response of these smart materials when subject to large strains. While uniaxial compression and tension, and simple shear tests have been performed to large strains [6–9], the variety of materials used in these experiments makes it difficult to compare results. In order to develop constitutive models able to accurately describe the complex behaviour of MREs comprehensive datasets are required. This involves testing both in the absence of and in the presence of magnetic fields, under various deformation modes, including multi-axial deformations, all on the same type of material [10, 11]. Fitting the parameters of complex constitutive models can be a challenging task and the challenge increases with the complexity of the constitutive model due to the increase of independent parameters within the model. For example, constitutive equations for incompressible isotropic materials depend on just two invariants [12]. Models for incompressible anisotropic materials depend on four invariants [13]. For incompressible magneto-sensitive anisotropic materials the constitutive model can depend on as many as nine invariants [14]. The number of independent parameters increases with the number of invariants; consequently, in order to uniquely

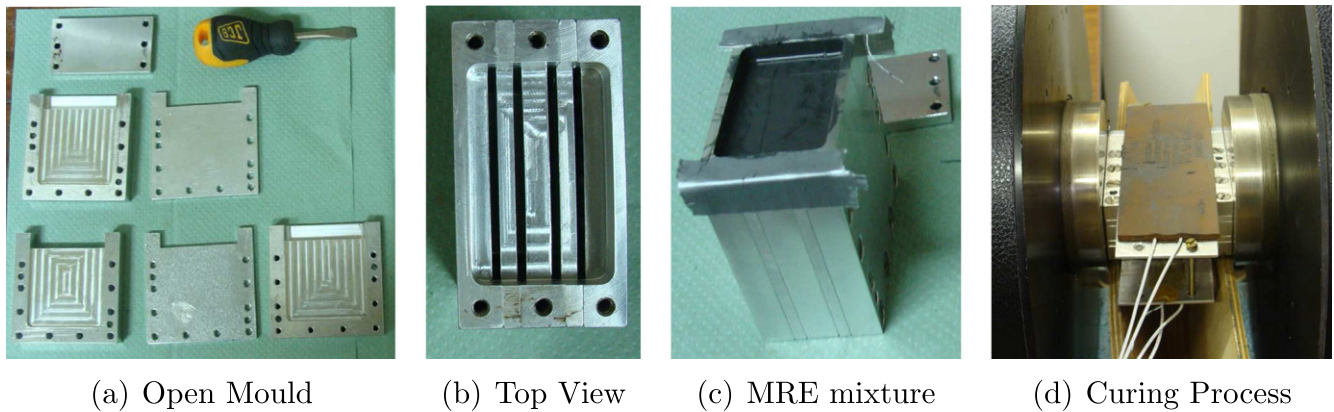| (a) Open Mould | (b) Top View | (c) MRE mixture | (d) Curing Process |

**Figure 1.** The moulds to manufacture samples for equi-biaxial tension tests. (a) Completely open, (b) ready for the pouring process, (c) with the MRE mixture inside, and (d) between the heater plates and in between the poles of the electromagnet during the curing process.

determine all the model parameters for such complex material behaviour, multiple independent experiments, each inducing different deformation modes, must be conducted. This requirement for multiple independent tests provides the motivation for the current investigation.

While Zhou [15] used the bubble-inflation method to study the fatigue behaviour of MREs in the absence of magnetic fields, so far the behaviour of MREs subject to multi-axial deformations in the presence of applied magnetic fields has yet to be studied. In this research, the response of MREs has been studied under equi-biaxial tension up to 10% strain. A bespoke test rig was designed to facilitate testing using a standard universal test machine. Both isotropic and anisotropic MREs with 10%, 20%, and 30% volume particle concentration were studied in the absence and in the presence of a 67.5 mT magnetic field applied parallel and perpendicular to the direction of particle alignment in anisotropic MREs. Full-field strains were measured optically across the samples using a digital image correlation (DIC) system, and the magnetic field distribution was simulated using the commercial finite element software *Comsol*. Analysis of the principal stresses in the experiments is based on assumptions verified previously by uniaxial tension tests on the same type of material [16] and by the calculated distribution of the magnetic field strength [17]. These assumptions are improved compared to those used in an earlier published conference paper [18]. The stress–strain results and the magneto-rheological (MR) effect, defined as the increase in tangent moduli due to an applied field, are both reported. Together with large-strain compression, tension and pure shear tests performed on the same type of material [16], a set of experimental data is presented that characterizes MREs under several deformation modes up to considerably large strain. This is an essential basis for the development of accurate constitutive models for MREs.

## 2. Materials

Silicone rubber *MM 240TV* mixed with 30 w% silicone oil *ACC 34*, both purchased from the company ACC Silicones

were used as the elastomeric matrix material. Carbonyl iron particles provided by the company BASF were used as the magnetic particles; the type SQ was chosen with an average particle size from 3.7 to 4.7 $\mu$m. Isotropic and anisotropic MREs with volume particle concentrations of 10%, 20% and 30% were prepared, together with specimens made simply of the pure matrix material, i.e. 0% particle volume concentration. The manufacturing process of a commercially available silicone rubber is straightforward; all the components were mixed thoroughly for three minutes with a hand mixer, and the mixture was degassed in a vacuum chamber for 10 min, both before and again after the mixture was poured in the moulds. The MREs were cured for 1.5 hours at 100 °C. To prepare anisotropic MREs the mixture inside the moulds was exposed to a 400 mT magnetic field during the curing process. Sample sheets with dimensions 50 × 50 × 2 mm were manufactured. The moulds used to prepare these samples were made of aluminium and brass to avoid any unwanted magnetization. The mould and the manufacturing process are illustrated in figure 1.

## 3. Test setup and procedure

Tests were performed on isotropic and anisotropic MREs with 10%, 20% and 30% iron content. A special test rig was designed to enable equi-biaxial testing using an universal test machine (Zwick Z250), which measured vertical force and displacement. Figure 2 shows an isotropic MRE specimen clamped in the rig. The rig was designed in accordance with the British Standard [11] and consisted of upper and lower frames, each attached to the test machine. The two frames were not connected and did not contact one another during the test. Test specimens were held in the rig using three sliding clamps on each side of the specimen; the clamps were free to move along the side length of the frame as the test proceeded, ensuring an almost uniform biaxial stretch of the MRE samples. To reduce friction and to avoid interactions between the test rig and the magnetic field, the rig and the sliding clamps were made of polytetrafluoroethylene (Teflon). The clamps for holding the rubber were made of aluminium with brass screws. The test rig did not allow strains larger than 10% due
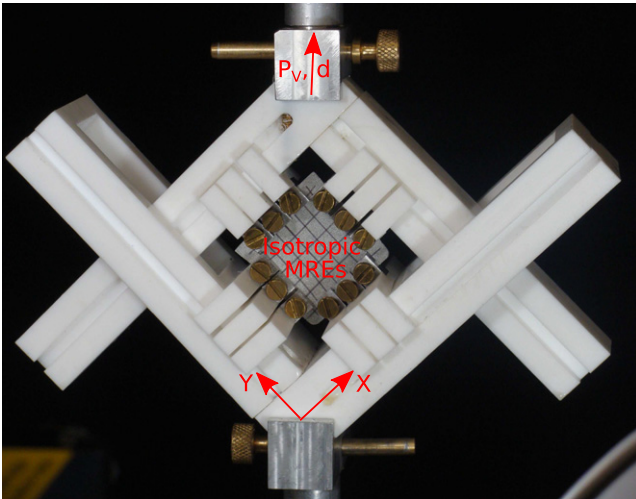
**Figure 2.** The biaxial test rig attached to the uniaxial test machine (Zwick Z250). An isotropic MRE in the absence of a magnetic field is illustrated (case 1). The vertical recorded load, $P_V$, the displacement, $d$, and the coordinate system are indicated.

to the clamping system and the soft materials used. 175 mm long aluminium connecting rods attaching the biaxial test rig to the Zwick test machine ensured sufficient distance between the permanent magnets, the load-cell and the steel parts of the test machine to ensure again any undesirable effects (such as false force readings). Four strong permanent neodymium N52 magnets, two placed on either side of the test rig, were used to create an average magnetic induction of 67.5 mT in the main direction and 7.1 mT perpendicular to this direction. The magnetic field was calculated using finite element analysis in the absence of an MRE sample (the field strength is expected to change once the sample is introduced in the setup). The inter-magnet distance of 140 mm was kept constant during all experiments. The permanent magnets and the direction of the particle alignment in an anisotropic MRE specimen are shown in figure 3. A naming convention is used when describing the different types of experiment. Case 1 is illustrated in figure 2 and case 2 to case 5 are illustrated in figure 3.
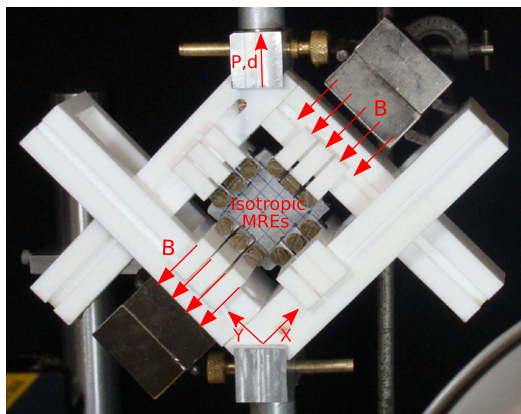


(a) CASE 2
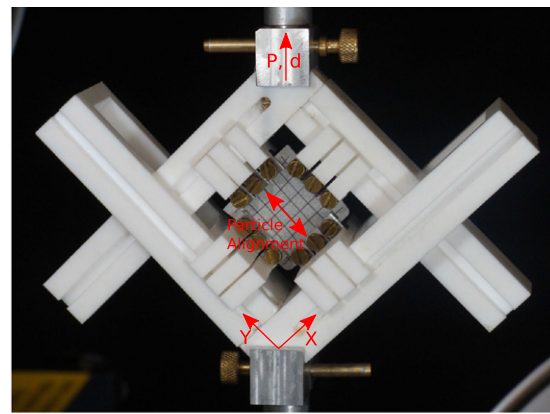


(b) CASE 3
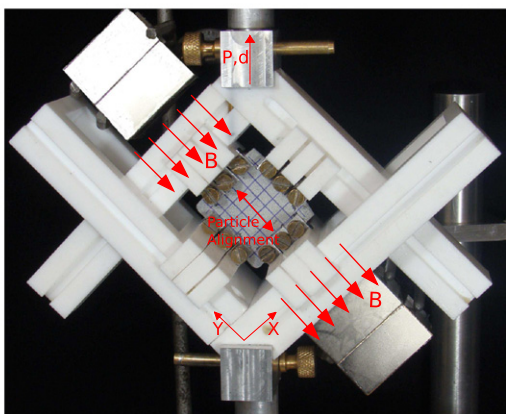


(c) CASE 4
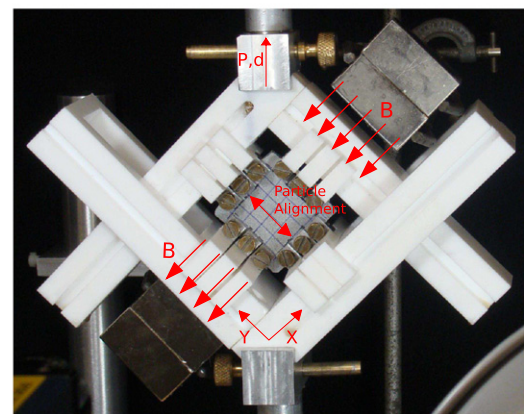


(d) CASE 5

**Figure 3.** Biaxial test setup with (a) an isotropic MRE with applied magnetic induction in the $x$-direction (case 2), (b) an anisotropic MRE with particle alignment in the $y$-direction without magnetic field (case 3), and with magnetic field (c) in the $y$-direction parallel to the particle alignment (case 4), and (d) in the $x$-direction perpendicular to the particle alignment (case 5).
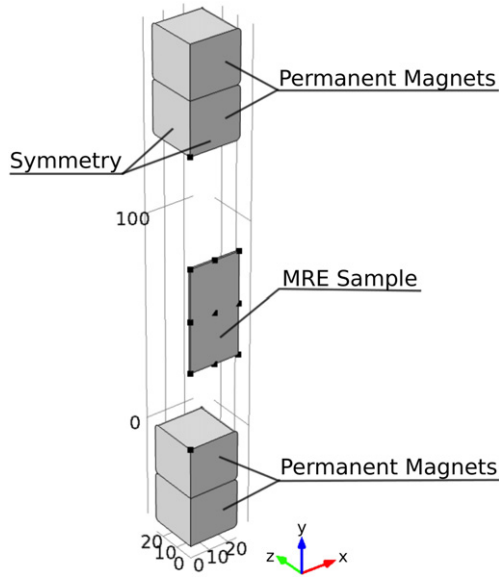
3

**Figure 4.** Geometry implemented in *Comsol* to calculate the distribution of the magnetic flux density in the biaxial test setup. Two magnets are placed on either side of the test rig with an inter-magnet distance of 140 mm in the *y*-direction.

The tests were conducted at a test speed of 10 mm min$^{-1}$ with up to 10 mm vertical displacements resulting in approximately 10% strain in the stretching directions. Anisotropic MREs with 30% iron particles were only stretched up to 7% strain due to tearing of samples at higher strains. MREs were first tested without an applied magnetic field, followed by tests with 67.5 mT in the main magnetic field direction. All tests were 4-cycle tests and the third loading cycle was used to analyse and interpret the stress–strain results. A DIC system (Limess) was used to measure full-field engineering strains within the MRE samples during the experiments. This measurement ensured that any additional strains that might be present in the test rig are excluded from the presented stress–strain results.

## 4. Distribution of the magnetic field strength

The magnetic flux distributions within the volume occupied by the MRE sample were simulated with the multi-physics software *Comsol* (AC/DC package) [19]. The model geometry is shown in figure 4; symmetry conditions meant that only one quarter of the setup was required in the model. The test rig itself was made of non-magnetic materials and had no influence on the magnetic flux calculations, and was thus not modelled. Average dimensions measured during the experiments on isotropic and anisotropic MREs were used in the model. Further information about the finite element model can be found in [17]. The simulation results are in excellent agreement with magnetic field strength measurements taken at various positions in the setup using a Gaussmeter (F.W. Bell Model 5180). Contrary to the actual experimental setup (see figure 3) the main magnetic field direction in the *Comsol* model was always the *y*-direction and the particle alignment direction of anisotropic MREs was rotated. This was done to simplify the modelling procedure.
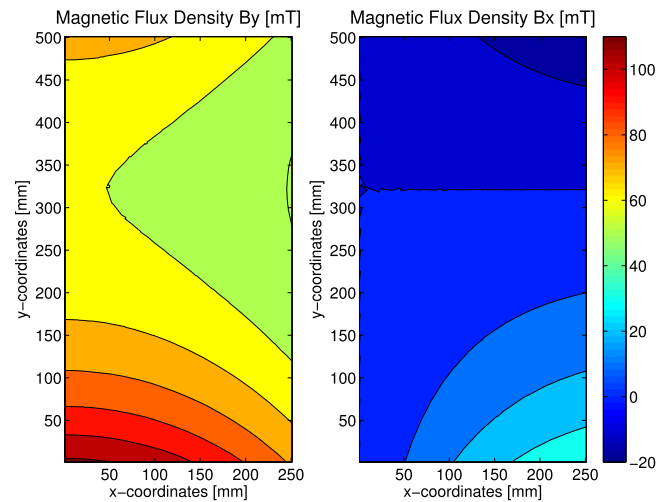


**Figure 5.** Magnetic flux density, $B_Y$ and $B_X$, within the volume of the MRE sample (calculated in the absence of a MRE sample with $\mu_r = 1$) with $B_{Y,\mathrm{mean}} = 67.5$ mT and $B_{X,\mathrm{mean}} = 7.1$ mT.

**Table 1.** Relative permeabilities for isotropic MREs, $\mu_{\mathrm{iso}}$, and for anisotropic MREs in the particle alignment direction, $\mu_\parallel$, and perpendicular to the alignment direction, $\mu_\perp$.

|                      | $\mu_{\mathrm{iso}} / \mu_\parallel$ | $\mu_\perp$ |
| -------------------- | :---: | :---: |
| Isotropic 10% MREs   | 1.60  |       |
| Isotropic 20% MREs   | 2.20  |       |
| Isotropic 30% MREs   | 3.70  |       |
| Anisotropic 10% MREs | 1.60  | 1.50  |
| Anisotropic 20% MREs | 2.70  | 2.30  |
| Anisotropic 30% MREs | 4.45  | 3.55  |

The magnetic flux density in the *x*- and *y*-directions has to be considered as the field strength in each direction influences the stiffness of the MRE sample in each of these directions [6]. The ratio of the magnetic field strength in the two orthogonal directions is used in analysing the results of the test and so some care has to be taken here to understand the field distribution. Since the biaxial test samples are square, a significant component of the magnetic flux exists perpendicular to the main magnetic flux direction. The distribution of the magnetic flux density, $B_Y$ and $B_X$, within the volume usually occupied by an MRE sample (but calculated in the absence of a sample, i.e. with $\mu_r = 1$) is shown as a contour plot in figure 5. The average value of $B_Y$ taken over the volume of the MRE sample is 67.5 mT, and the flux density in the *y*-direction differs across this volume by about 90.4%. In contrast, the average value of $B_X$ is only 7.1 mT, but undergoes a much greater variation in strength of up to 357.2%. The changes in the horizontal flux density, $B_X$, are therefore far larger than those in the vertical direction.

The magnetic flux distribution across the volume occupied by the MRE sample was also calculated in the presence of the samples ($\mu_r > 1$) by changing the material properties of the MRE samples in the finite element model. The magnetic permeability was defined as isotropic or anisotropic and values determined earlier [17] were used; those values are

**Table 2.** Mean values, $B_{\mathrm{mean}}$ [mT], and relative difference $100 \times (B_{\max} - B_{\min})/B_{\mathrm{mean}}$ (%), of the magnetic flux distribution, $B_Y = B_{\parallel}$, in the main magnetic field direction and, $B_X = B_{\perp}$, perpendicular to the main direction, within the volume occupied by isotropic and anisotropic MRE samples ($\mu_r \geqslant 1$). The ratio $B_{\parallel}/B_{\perp}$ [-] is calculated with $B_{\mathrm{mean}}$. Values for $B_{\perp}$ are calculated with absolute values.

| MRE Sample | Iron [%] | Flux in $y$-direction | | Flux in $x$-direction | | Ratio $B_{\parallel}/B_{\perp}$ |
|---|---|---|---|---|---|---|
| | | $B_{\mathrm{mean}}$ | $\frac{B_{\max} - B_{\min}}{B_{\mathrm{mean}}}$ | $B_{\mathrm{mean}}$ | $\frac{B_{\max} - B_{\min}}{B_{\mathrm{mean}}}$ | |
| Pure rubber | 0 | 67.53 | 90.4 | 7.09 | 357.2 | 9.52 |
| Isotropic MREs | 10 | 103.95 | 80.3 | 10.47 | 328.4 | 9.93 |
| | 20 | 138.45 | 82.1 | 13.27 | 324.8 | 10.43 |
| | 30 | 217.74 | 85.3 | 18.61 | 352.1 | 11.69 |
| Anisotropic MREs aligned in $y$-direction | 10 | 104.53 | 77.2 | 9.9 | 289.3 | 10.58 |
| | 20 | 167.20 | 80.6 | 13.35 | 296.6 | 12.52 |
| | 30 | 257.03 | 83.6 | 17.16 | 306.1 | 14.98 |
| Anisotropic MREs aligned in $x$-direction | 10 | 97.62 | 83.0 | 11.16 | 329.0 | 8.75 |
| | 20 | 143.10 | 85.7 | 16.66 | 338.6 | 8.59 |
| | 30 | 208.12 | 87.9 | 23.20 | 358.7 | 8.97 |

listed in table 1. Results of the finite element calculations for each type of MRE are summarized in table 2. The average magnetic flux densities and the differences in the flux across the volume occupied by the MRE sample are provided as well as the ratio between $B_Y = B_{\parallel}$ in the main magnetic field direction and $B_X = B_{\perp}$ perpendicular to it. The terms $B_{\parallel}$ and $B_{\perp}$ are introduced to avoid confusion in section 6. The factor $B_{\parallel}/B_{\perp}$ is largest at 14.98 (when the magnetic field is applied parallel to the direction of particle alignment), and is smallest at 8.59 (when the magnetic field is applied perpendicular to the alignment direction).

## 5. Optical strain measurement

A DIC system (Limess) was used to measure the strains. The system consists of 4 M pixel cameras, bulb lights, and the *VIC 3D* software to perform the analysis. Test samples were sprayed with a white random speckle pattern; images of the samples are shown in figures 2 and 3. Grid lines were also drawn on the samples to enable manual calculation of the strains by measuring pixel positions using the software *ImageJ*. A series of images was recorded during the cyclic tests. The DIC software performed correlation analysis by comparing the defined area of interest (AoI) in each image. The AoI was defined on the MRE sample as a square area situated in the centre. The software divides the pattern into smaller areas and follows the same areas in each image. During the test, the speckle pattern is stretched and displaced. By tracking the speckle pattern, the DIC software is able to calculate displacements and strains across the test sample. The output of the DIC software are matrices containing values of displacement and engineering strain in both the $x$ and $y$-direction at each point in the AoI at any given time. Confidence values describing the match at each point are also provided. The engineering strains in the $x$-direction of a pure

rubber sample are shown in figure 6(a). DIC data were post-processed using *Matlab*. The AoI was cropped, and also rotated for better handling. Unreliable values were eliminated using the confidence values provided by the DIC software. The post-processed strain field is shown in figure 6(b). The strains in the $x$-direction within the post-processed AoI are relatively uniform, differing between 8.6% and 10.2%. Mean values and standard deviations of the post-processed strain field are calculated and plotted versus time in figure 7, where the strain in both the local $x$- and $y$-directions are shown to be in excellent agreement. Mean values of the original AoI and of the cropped strain field were compared and do agree; however the standard deviations in strains resulting from the original AoI (see figure 6(a)) are larger than those shown in the processed AoI (see figure 6(b)). The strains in the $x$- and $y$-directions are nearly identical; this implies that the frame structure is rigid enough to impose equi-biaxial deformation kinematics. This was also found to be the case even for anisotropic MREs with higher iron content. The load–displacement data recorded by the test machine are subsequently related to the strain–time data of the DIC analysis via the time recorded by the test machine.

## 6. Stress calculation

Only the vertical force, $P_V$, was recorded by the uniaxial test machine. In order to calculate stresses in the two stretching directions, the structural system of the biaxial test has to be analysed and several assumptions have to be made. The biaxial rig is assumed to be a rigid body with the top frame moving 10 mm in the vertical direction; the experiment was displacement controlled. This movement of the rig caused stresses within the soft rubber. The structural system is illustrated in figure 8. The rigid body assumption of the biaxial frame is supported by the optical strain measurement which confirmed
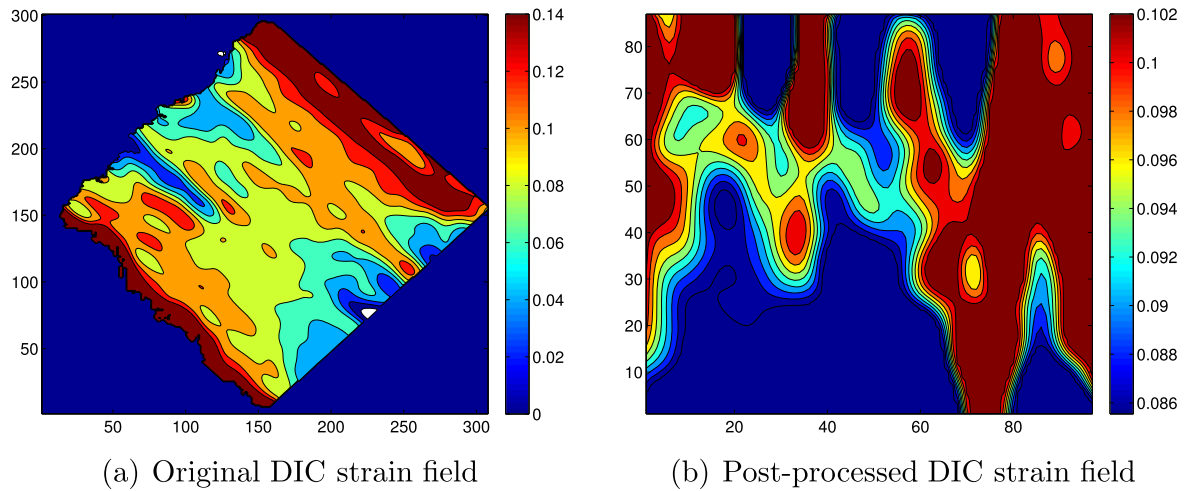
(a) Original DIC strain field (b) Post-processed DIC strain field

**Figure 6.** Maximum strain in the *x*-direction in the third loading part of a pure rubber sample calculated by the DIC software. (a) Original strain field as calculated by the DIC software and (b) rotated strain field, after unreliable values were eliminated and borders cropped.
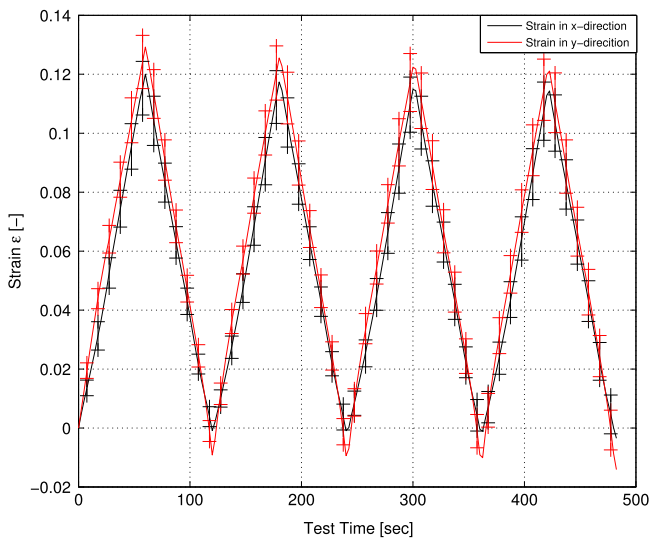


**Figure 7.** Engineering strain of a pure rubber sample in both stretching directions versus time. Mean values and standard deviations of the post-processed DIC field of the four-cycle test are illustrated.



$P_V$ ... Vertical Force recorded by the test machine
$P_H$, M ... Horizontal force and moment, not recorded by the test machine
σx, σy ... Engineering stress in the MRE samples
w ... Length where the sample is clamped

**Figure 8.** Structural system of the biaxial test setup used to calculate stresses within the MRE sample.

equal strains in both stretching directions. Rotation of the biaxial frame was prevented by its connection with the test machine. The forces, $P_V$ and $P_H$, and the moment, $M$, were generated at the fixed support but only the vertical force, $P_V$, was recorded by the test machine. The stresses are assumed to be equally distributed across the length of the three clamps $w$ holding the side of the MRE samples. The distance $a$ is the distance between the fixed support and the clamps. The stresses are calculated in the reference configuration. To derive the equations for the stresses, $\sigma_X$ and $\sigma_Y$, five cases are distinguished (case 1 to case 5 as illustrated in figures 2 and 3). The analysis of each case is presented in the following sections.

### 6.1. Case 1—isotropic MREs without magnetic field

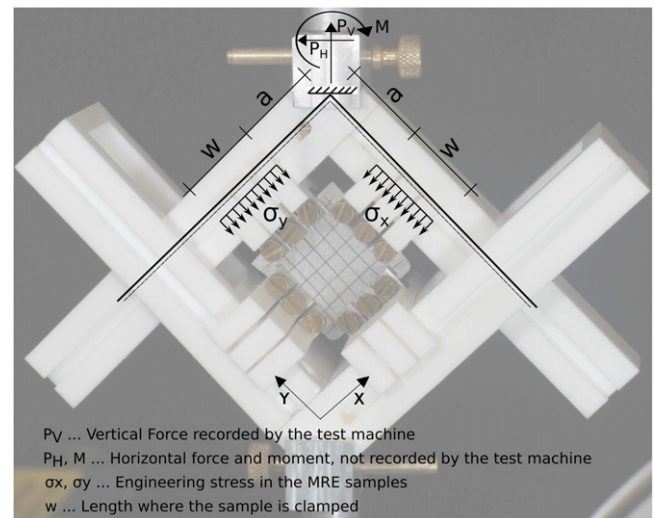Isotropic MREs are supposed to have equal properties in all directions, which implies that the stresses $\sigma_X$ and $\sigma_Y$ are

identical. Figure 2 shows the setup of case 1. From equilibrium of stresses in the *x*- and *y*-directions, the stresses can be calculated as,

$$\sigma_X = \sigma_Y = \frac{P_V}{\sqrt{2} \cdot t \cdot w} \qquad (1)$$

with the vertical force, $P_V$, the thickness of the sample, $t$, and the width of the clamps, $w$. As the horizontal force $P_H$ and the moment $M$ at the fixed support are zero, no assumptions are required in analysing case 1.

### 6.2. Case 2—isotropic MREs with magnetic induction in the x-direction

The magnetic field is assumed to change the stiffness of the MRE in the *x*- and *y*-directions by the same ratio as that between the average magnetic induction in the two directions $B_\parallel/B_\perp$ (see table 2). The setup of case 2 is shown in figure 3(a). When a magnetic induction is applied on the

isotropic MREs, the force measured in the vertical direction, $P_V$, is larger than the force measured on isotropic MREs without an applied induction $P_{V,CASE1}$. The increase, $P_{inc} = P_V - P_{V,CASE1}$, is attributed to increases in the force generated in the two stretching directions. The relation between the stresses $\sigma_{x,inc}$ and $\sigma_{y,inc}$ due to $P_{inc}$ is determined by the factor $B_\parallel / B_\perp$ with $B_\parallel$ acting in the $x$-direction:

$$\frac{\sigma_{x,inc}}{\sigma_{y,inc}} = \frac{B_\parallel}{B_\perp}. \tag{2}$$

Equation (2) is a significant assumption, and other more complex non-linear descriptions, such as $\sigma_{x,inc}/\sigma_{y,inc} = \left(B_\parallel/B_\perp\right)^\alpha$ could be more appropriate. Here $\alpha$ is a parameter that should be determined through more experiments. Nevertheless, in order to simplify the subsequent analysis and also because of the time constraints governing this investigation, the assumption of equation (2) is currently a necessary concession. Attention is drawn to this point as a possible source of error in the method and work to clarify the accuracy of this assumption is deferred to the future. For example, uniaxial tension tests with the particle alignment in the loading direction but with a magnetic field perpendicular to the loading direction could be conducted to examine the accuracy of equation (2). With the relation of equation (2) and the equilibrium of forces in the vertical direction the stress definitions can be derived as,

$$\sigma_X = \sigma_{x,CASE1} + \sigma_{x,inc} = \frac{P_{V,CASE1}}{\sqrt{2} \cdot t \cdot w}$$
$$+ \frac{\sqrt{2}\left(P_V - P_{V,CASE1}\right)}{\left(\frac{B_\perp}{B_\parallel} + 1\right) \cdot t \cdot w}, \tag{3}$$

$$\sigma_Y = \sigma_{y,CASE1} + \sigma_{y,inc} = \frac{P_{V,CASE1}}{\sqrt{2} \cdot t \cdot w}$$
$$+ \frac{\sqrt{2}\left(P_V - P_{V,CASE1}\right)}{\left(\frac{B_\parallel}{B_\perp} + 1\right) \cdot t \cdot w}. \tag{4}$$

The value $P_{V,CASE1}$ is the mean value of forces measured on isotropic MREs of the same iron particle volume fraction tested without an applied field. Note, the horizontal force $P_H$ and the moment $M$ are not zero in this and in all following cases.

### 6.3. Case 3—anisotropic MREs without magnetic field

The particle alignment direction of the anisotropic MREs was oriented in the $y$-direction for all tests. The setup of case 3 is illustrated in figure 3(b). These MREs are much stiffer in the particle alignment direction, and the stresses in the $y$-direction are therefore higher than in the $x$-direction, i.e. $\sigma_Y > \sigma_X$. As only the vertical force, $P_V$, was measured by the test machine, an assumption is required in order to attribute the vertical force to the two stretching directions. In uniaxial tension tests [16], measurements on anisotropic MREs with the particle
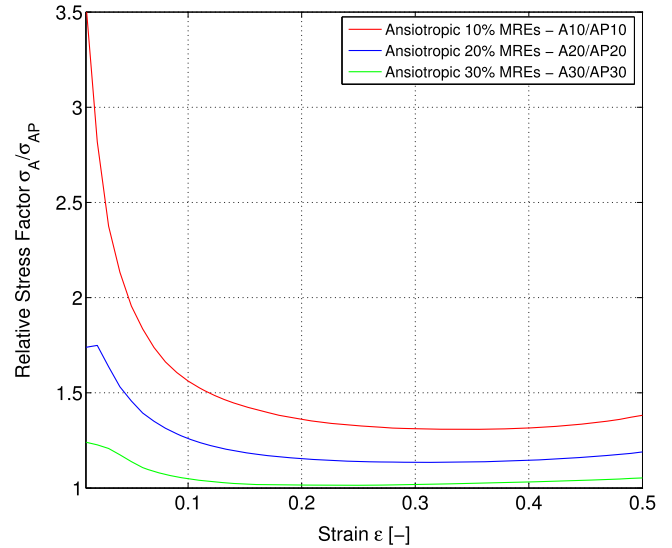


**Figure 9.** Relative stress factor $f(\varepsilon)$ between anisotropic MREs with alignment in (A) and perpendicular to (AP) the loading direction tested in uniaxial tension are shown. The stress factor is plotted versus the engineering strain in the uniaxial stretching direction. Note that the stress factor tends to infinity for small strains, so values below 2% strain are unreliable.

alignment in the loading direction (A) and perpendicular to it (AP) were performed. The relative stress factor between stresses of anisotropic samples with alignment in the loading direction, $\sigma_A$, and perpendicular to the loading direction, $\sigma_{AP}$, is used to evaluate the relationship between $\sigma_X$ and $\sigma_Y$ in the equi-biaxial tension tests. In the case of biaxial tension test both directions are the loading directions, thus in the $y$-direction the particle alignment is parallel and in the $x$-direction the alignment is perpendicular to the load:

$$f(\varepsilon) = \frac{\sigma_A(\varepsilon)}{\sigma_{AP}(\varepsilon)} = \frac{\sigma_Y}{\sigma_X}. \tag{5}$$

Mean values from at least three repeated uniaxial tension tests were taken to calculate the relative stress factors. These are plotted versus uniaxial strain in figure 9. With the stress factor defined in equation (5), combined with the equilibrium condition, the stresses in both stretching directions can be calculated as,

$$\sigma_X = \frac{\sqrt{2} \cdot P_V}{(f(\varepsilon) + 1) \cdot t \cdot w}, \tag{6}$$

$$\sigma_Y = \frac{\sqrt{2} \cdot P_V \cdot f(\varepsilon)}{(f(\varepsilon) + 1) \cdot t \cdot w}. \tag{7}$$

This method of using the relative stress factor obtained from uniaxial tension tests provides a first approximate analysis of the biaxial test data. It might be possible in future to improve the analysis method by using results of constitutive modelling. For now, however, this is the only information available to describe the behaviour of anisotropic MREs.

### 6.4. Case 4—anisotropic MREs with magnetic induction in the y-direction

Anisotropic MREs with particle alignment in the y-direction were tested with a magnetic induction also applied in the y-direction, thus the direction of the particle alignment was parallel to the main magnetic field direction; the setup is shown in figure 3(c). Two assumptions are required to analyse the test results of case 4.

(i) The force $P_V$ increases due to the applied magnetic induction by $P_{V,\text{inc}}$; thus $P_V = P_{V,\text{CASE3}} + P_{V,\text{inc}}$. The increased force, $P_{V,\text{inc}}$, can be attributed to the two stretching directions in the same way as in case 2. The only difference here is that the magnetic field is now applied in the y-direction rather than in the x-direction. The relation between the magnetic factor $B_\parallel/B_\perp$ and the stresses $\sigma_X$ and $\sigma_Y$ of the biaxial tests are thus defined as follows:

$$\frac{\sigma_{y,\text{inc}}}{\sigma_{x,\text{inc}}} = \frac{B_\parallel}{B_\perp}. \tag{8}$$

(ii) The stresses resulting from $P_{V,\text{CASE3}}$ (equations (6) and (7)) were calculated with a stress factor $f(\varepsilon)$ obtained from uniaxial tension tests.

The resulting stresses $\sigma_X$ and $\sigma_Y$ are defined in equations (9) and (10). As both the particle alignment and the applied magnetic field are in the y-direction, the stresses in this direction are expected to be much higher than the stresses in the x-direction, i.e. $\sigma_Y \gg \sigma_X$,

$$\sigma_X = \sigma_{x,\text{CASE3}} + \sigma_{x,\text{inc}} = \frac{\sqrt{2} \cdot P_{V,\text{CASE3}}}{(f(\varepsilon) + 1) \cdot t \cdot w}$$
$$+ \frac{\sqrt{2}\left(P_V - P_{V,\text{CASE3}}\right)}{\left(\frac{B_\parallel}{B_\perp} + 1\right) \cdot t \cdot w}, \tag{9}$$

$$\sigma_Y = \sigma_{y,\text{CASE3}} + \sigma_{y,\text{inc}} = \frac{\sqrt{2} \cdot P_{V,\text{CASE3}} \cdot f(\varepsilon)}{(f(\varepsilon) + 1) \cdot t \cdot w}$$
$$+ \frac{\sqrt{2}\left(P_V - P_{V,\text{CASE3}}\right)}{\left(\frac{B_\perp}{B_\parallel} + 1\right) \cdot t \cdot w}. \tag{10}$$

### 6.5. Case 5—anisotropic MREs with magnetic induction in the x-direction

Case 5 is very similar to case 4, with the only difference that the magnetic induction is applied in the x-direction rather than in the y-direction. The setup of case 5 is shown in figure 3(d). The assumptions and the derived equations are analogous to

those explained in case 4:

$$\sigma_X = \sigma_{x,\text{CASE3}} + \sigma_{x,\text{inc}} = \frac{\sqrt{2} \cdot P_{V,\text{CASE3}}}{(f(\varepsilon) + 1) \cdot t \cdot w}$$
$$+ \frac{\sqrt{2}\left(P_V - P_{V,\text{CASE3}}\right)}{\left(\frac{B_\perp}{B_\parallel} + 1\right) \cdot t \cdot w}, \tag{11}$$

$$\sigma_Y = \sigma_{y,\text{CASE3}} + \sigma_{y,\text{inc}} = \frac{\sqrt{2} \cdot P_{V,\text{CASE3}} \cdot f(\varepsilon)}{(f(\varepsilon) + 1) \cdot t \cdot w}$$
$$+ \frac{\sqrt{2}\left(P_V - P_{V,\text{CASE3}}\right)}{\left(\frac{B_\parallel}{B_\perp} + 1\right) \cdot t \cdot w}. \tag{12}$$

Again, two assumptions are used to calculate the stresses in the two stretching directions: the uniaxial stress factor (equation (5)) and the magnetic factor (equation (2)).

The assumptions used here are improved compared to an earlier published conference paper [18]. In particular, the stress factor obtained from uniaxial tension tests performed in [16] and used here to interpret the experimental data, is a function of strain rather than of displacement. Further, the magnetic field assumption is based on a factor between the average levels of magnetic induction in the two stretching directions instead of assuming changes in material behaviour only in the direction of the magnetic field. These modifications provide improved accuracy and reliability when interpreting the results.

## 7. Stress–strain results and MR effect

The experimental results from tests on isotropic and anisotropic MREs conducted in the absence of a magnetic field (case 1 and case 3), and those conducted in the presence of magnetic field (case 2, case 4 and case 5) are reported in this section.

The load–displacement data recorded by the uniaxial test machine are converted to stress–strain data in the two stretching directions (X and Y) using the optically measured strains described section 5 and the stress equations derived in section 6. First, the MRE behaviour in the absence of a magnetic field is discussed. The effect of changing the iron particle volume concentration is considered and the differences between the isotropic and anisotropic MREs is ascertained.

Second, the MR effect is studied by comparing stress–strain results of tests conducted in the absence of magnetic fields with those conducted in the presence of magnetic fields. The increase in the tangent moduli versus large-strain is reported for various applied magnetic field strengths. Absolute and relative MR effects are defined as

$$\text{MR}_{\text{abs}} = E_M - E_0 \tag{13}$$

$$\text{MR}_{\text{rel}} = E_M/E_0 \tag{14}$$

or expressed as the MR increase with $(E_M/E_0 - 1) \times 100$ defined as a percentage value. In these equations $E_0$ and $E_M$ are the tangent moduli calculated as the linear slope of the

(a) Load-Displacement Data
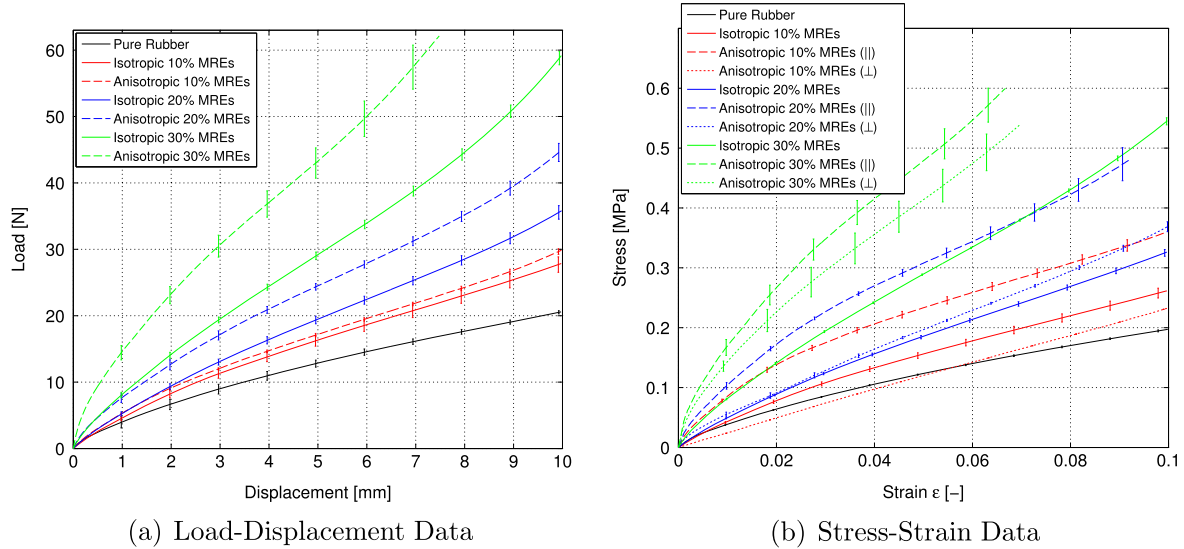


(b) Stress-Strain Data

**Figure 10.** Vertical load–displacement curve and the stress–strain curves comparing the different types of MRE samples tested in the absence of a magnetic field. Stresses of the isotropic MREs are compared with the stresses parallel ($\parallel$) and perpendicular ($\perp$) to the particle alignment of anisotropic MREs.



(a) $E_0$ versus strain
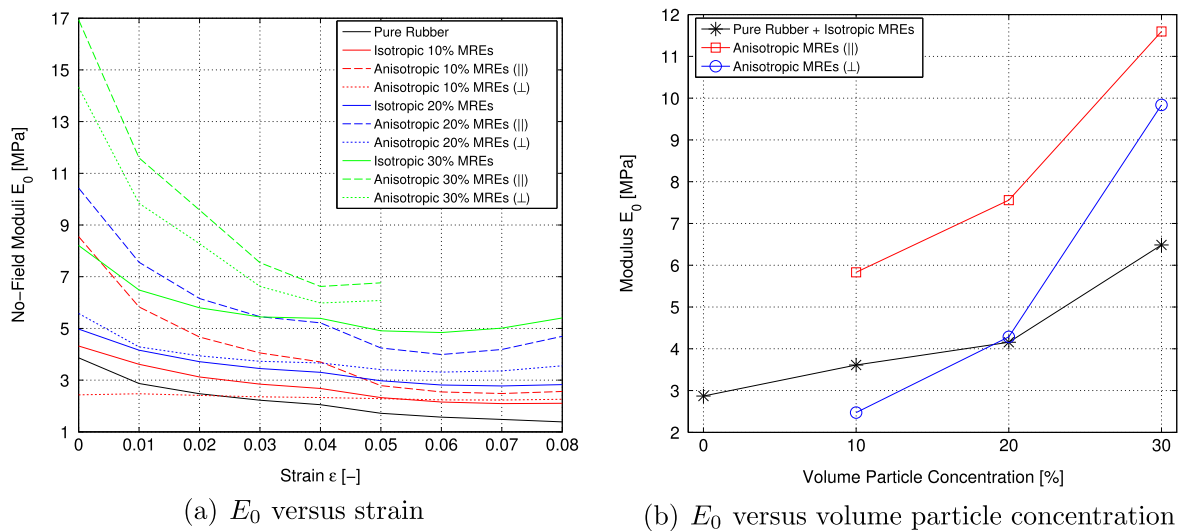


(b) $E_0$ versus volume particle concentration

**Figure 11.** Tangent moduli, $E_0$, versus the iron volume fraction of isotropic MREs and anisotropic MREs parallel ($\parallel$) and perpendicular ($\perp$) to the particle alignment direction. Tangent moduli between 1% and 2% strain are provided.

stress–strain curves (using 1% strain increments), from tests in the absence and in the presence of a magnetic field, respectively. Use of this small strain increment produces a reasonable approximation of the first derivative of the stress–strain curves.

### 7.1. Results of tests in the absence of a magnetic field (cases 1 and 3)

The vertical load versus displacement data for all types of MREs tested in the absence of a magnetic field are shown in figure 10(a). The measured force increases with increasing iron content. Also, forces are larger in anisotropic MREs compared to the equivalent isotropic MREs, and this difference increases with increasing iron particle volume

concentration. The associated stress–strain curves are shown in figure 10(b). In the case of anisotropic MREs the assumption discussed in section 6.3 has been applied. The tangent moduli, $E_0$, are plotted versus engineering strain in figure 11(a), and the maximum values between 1% and 2% strain are plotted versus the iron volume fraction in figure 11(b). The moduli increase in a non-linear manner with increasing iron volume content, where the MREs containing 30% iron particles exceed the linear level.

### 7.2. Characterization of the MR effect (cases 2, 4 and 5)

A magnetic field strength of 67.5 mT was applied in the main magnetic field direction to study the increase in stiffness of the MRE material in the equi-biaxial tension test series. The
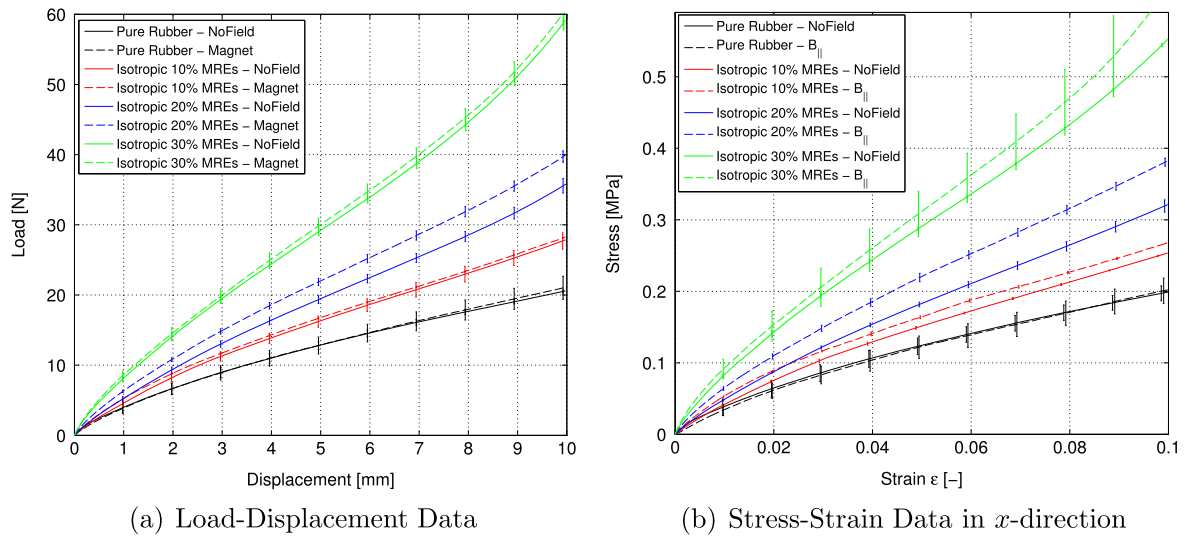
(a) Load-Displacement Data                    (b) Stress-Strain Data in $x$-direction

**Figure 12.** Vertical load–displacement and stress–strain curves in the $x$-direction of pure rubber and isotropic MRE samples with 10%–30% iron content comparing the *NoField* with the *Magnet* tests. The magnetic field, $B_{\parallel}$, was applied in the $x$-direction.

magnetic flux lines were not unidirectional; when interpreting experimental data, this issue is taken into account using the analysis described in section 6.

*Pure rubber and isotropic MREs* (*case 2*). The vertical force–displacement and the stress–strain data of isotropic MREs both with and without an applied magnetic flux are shown in figure 12. The stress–strain data in the direction of the applied magnetic field ($x$-direction) were calculated using equations (3) and (4). An increase in force is apparent when samples are subjected to a magnetic flux density, but this increase is most significant for isotropic MREs with 20% iron content.

The relative MR effects (equation (14)) of pure rubber and isotropic MREs are plotted versus engineering strain in figure 13. The highest relative MR increase of about 25% (1.09 MPa absolute MR effect) was achieved with an isotropic 20% MRE in the small-strain region. The isotropic 30% MREs exhibit lower relative increases of about 21%; this is a somewhat unexpected result but is probably due to the large no-field modulus of the isotropic 30% MRE specimens (see figure 11). As expected, the MR effects in the direction perpendicular to the applied induction are all close to 1. Results from pure rubber samples indicate an experimental and analytical error of about 3%.

*Anisotropic MREs* (*case 4 and case 5*). The load–displacement and the stress–strain curves of anisotropic MREs with magnetic field applied parallel to the direction of particle alignment are compared with those of the *NoField* tests in figure 14. All of the samples show an increase in force. Stresses are calculated using equations (9) and (10). Large increases in stress are visible for anisotropic MREs with 20% and 30% iron content. The relative MR effects are evaluated together with anisotropic MREs where the magnetic field is applied perpendicular to the alignment direction in figure 16.

The vertical load–displacement and stress–strain data of anisotropic MREs tested with a magnetic field applied perpendicular to the direction of particle alignment are shown in
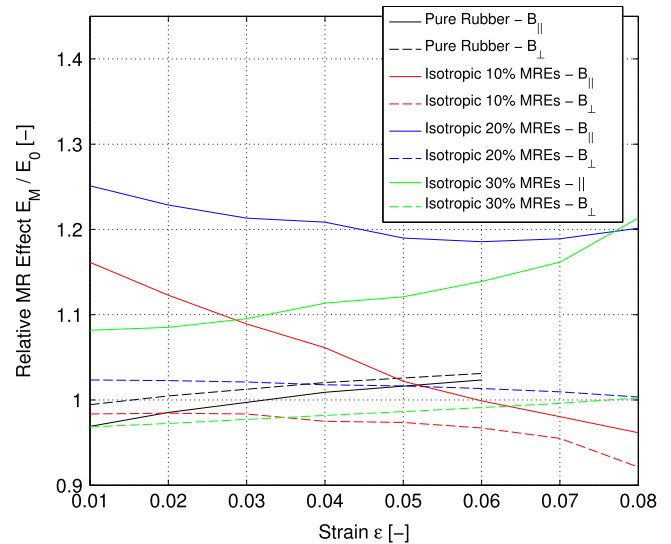


**Figure 13.** Relative MR effects of pure rubber and isotropic MREs with 10%–30% iron content are plotted versus strain. The magnetic field, $B_{\parallel}$, is applied in the $x$-direction.

figure 15. Increases in the forces are small for MREs with 10% and 30% iron content and are relatively large in the case of the anisotropic 20% MREs. The stresses in the two principal stretching directions are found using equations (11) and (12), and show the same tendency as the load–displacement data.

The relative MR effects of anisotropic MREs with the magnetic field applied parallel and perpendicular to the particle alignment direction are plotted versus strain in figure 16. The highest MR increase of about 74% (4.89 MPa absolute MR effect) was measured for the anisotropic MREs with 30% iron content when the magnetic field was applied parallel to the particle alignment direction. This MR increase occurred at about 4% strain, whereas in the small-strain region the increase measured on the same MRE was just 27.9%. The steep increase in MR effect of the anisotropic 30% MREs
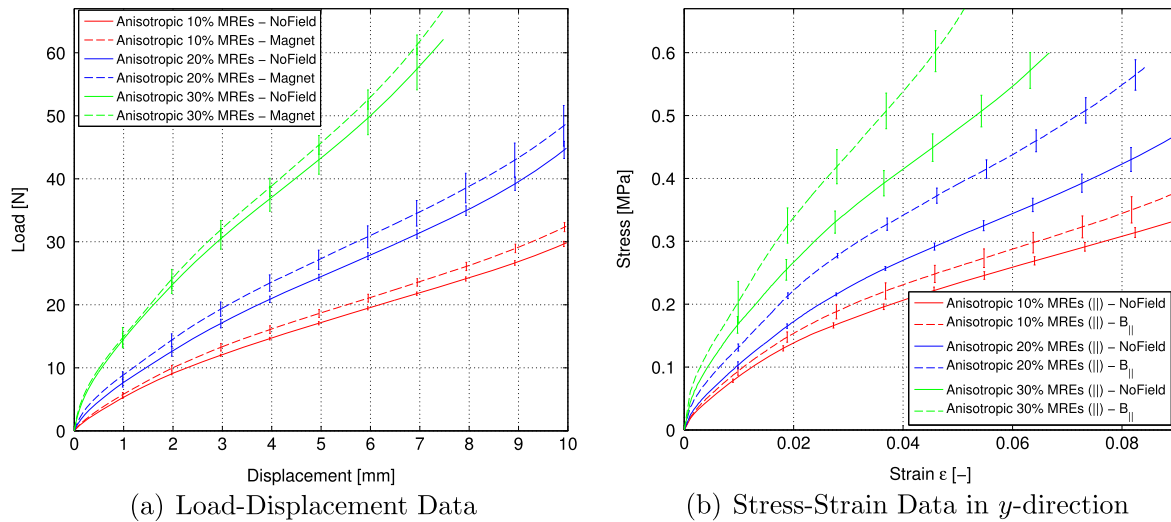
(a) Load-Displacement Data

(b) Stress-Strain Data in $y$-direction

**Figure 14.** Vertical load–displacement and stress–strain curves in the $y$-direction of anisotropic MREs with 10%–30% iron content comparing the *NoField* with the *Magnet* tests. Both the particle alignment and the applied magnetic induction, $B_{\|}$, were in the $y$-direction.
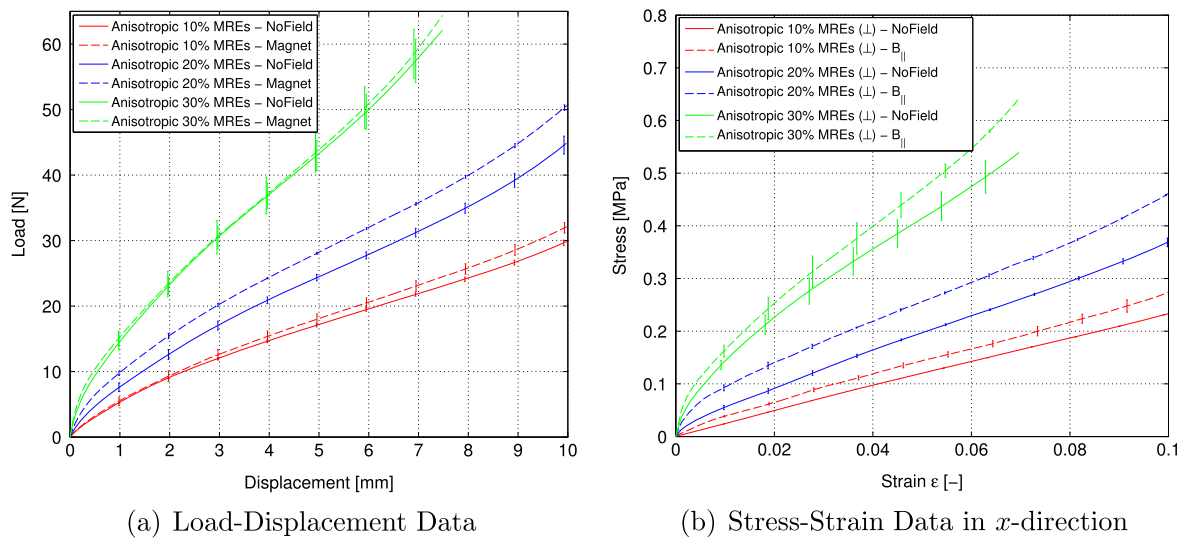


(a) Load-Displacement Data

(b) Stress-Strain Data in $x$-direction

**Figure 15.** Vertical load–displacement and stress–strain curves in the $x$-direction of anisotropic MREs with 10%–30% iron content comparing the *NoField* with the *Magnet* tests. The particles in the MREs were aligned in the $y$-direction while the magnetic induction, $B_{\|}$, was applied in the $x$-direction.

with increasing strain is unusual and contrasts with results found in uniaxial compression and tension experiments [16]. Nevertheless an increase in MR effect with increasing strain is observed in all MREs containing 30% particle content in this investigation (see figures 13 and 16(b)). It is not yet clear if this is a real effect or if due to either experimental error or errors due to the assumptions used in the analysis of the results. Further testing, or perhaps numerical modelling at the micro-scale e.g. [20] would be useful in clarifying this point. The MR effects perpendicular to the main magnetic field direction are all close to 1.

When the magnetic field was applied perpendicular to the particle alignment direction, the highest MR increase of 46% (2.24 MPa absolute MR effect) was achieved with MREs containing 20% iron content. The MR effects of anisotropic MREs with 10% and 20% iron content exceed the MR effects

found when the magnetic flux was applied parallel to the direction of particle alignment. This contrasts with the results found in uniaxial tension tests [16] and might be due to non-uniformity of the applied magnetic field. The results achieved in equi-biaxial tension are also influenced by the assumptions which were required to analyse the data, and could be improved with the use of constitutive modelling in future investigations.

*MR effect versus volume particle concentration.* To study the influence of the iron content, the maximum absolute and relative MR effects are plotted versus iron particle volume concentration in figure 17, and are also listed together with the no-field moduli $E_0$ and the field moduli $E_M$ in table 3. Only the MR effects in the main magnetic field direction are presented. MR effects increase with increasing iron content in the MRE samples, but the results of isotropic and anisotropic
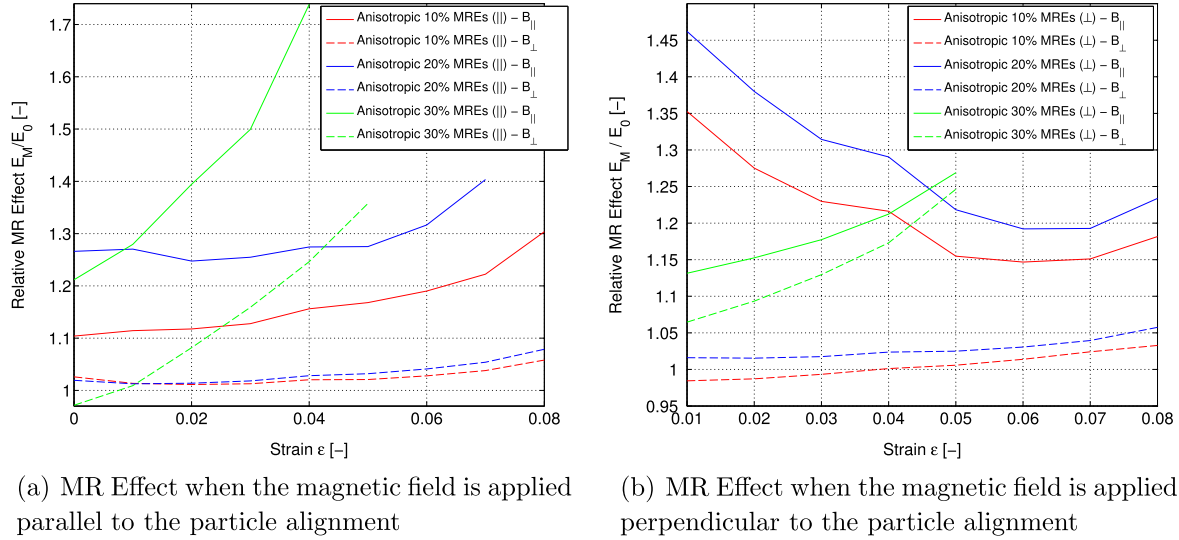
(a) MR Effect when the magnetic field is applied parallel to the particle alignment

(b) MR Effect when the magnetic field is applied perpendicular to the particle alignment

**Figure 16.** Relative MR effects of anisotropic MREs with 10%–30% iron content are plotted versus strain. The magnetic field, $B_{\parallel}$, is applied (a) in the $y$-direction (parallel to the direction of particle alignment), and (b) in the $x$-direction (perpendicular to the direction of particle alignment).



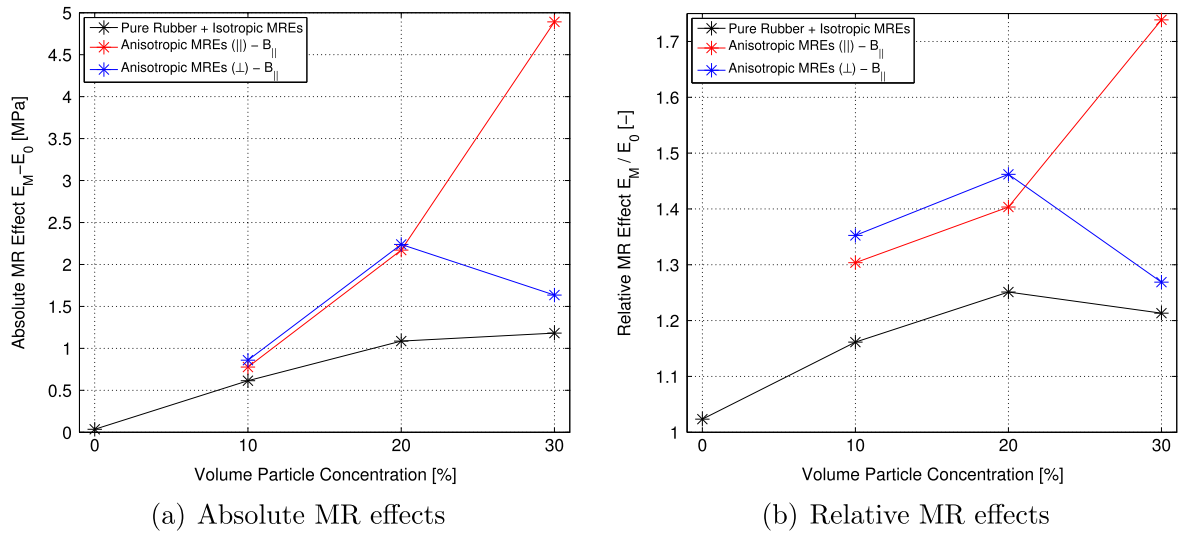(a) Absolute MR effects

(b) Relative MR effects

**Figure 17.** Maximum absolute and relative MR effects in the direction of the applied magnetic induction of all types of MREs versus the volume particle concentration.

MREs containing 30% iron content are somewhat unexpected, as discussed earlier.

## 8. Summary and conclusions

Equi-biaxial tension tests were performed on MREs. A special test rig was designed to enable testing on a universal test machine. Two permanent magnets on each side of the test rig created a magnetic flux density of 67.5 mT in the main magnetic field direction. Tests on isotropic and anisotropic MREs with 10%–30% iron particle content were performed with the magnetic field aligned both parallel and perpendicular to the particle alignment direction. A DIC system was used to measure full-field strains. To calculate stresses in the

two stretching directions, several assumptions were employed in the data analysis:

  (i) Frictionless clamps; forces along the frame axes are zero.
 (ii) The magnetic field changes the properties of the material parallel and perpendicular to the magnetic field direction by the same ratio as the ratio of mean magnetic field strengths in the two directions, $B_{\parallel}/B_{\perp}$.
(iii) For anisotropic MRE samples the relation between stresses parallel and perpendicular to the particle alignment is the same as a relative stress factor $f(\varepsilon)$ taken from uniaxial tension tests [16].

High MR increases of about 74% were found in anisotropic MREs containing 30% iron content when the particle

**Table 3.** No-field moduli $E_0$, the field moduli $E_M$, together with the maximum absolute and relative MR effects measured with magnetic induction parallel (∥) and perpendicular (⊥) to the particle alignment direction are listed. Only the MR effects in the main magnetic field direction are presented.

| MRE sample | Iron (%) | $E_0$ | $E_M$ | $MR_{abs}$ | $MR_{rel}$ |
|---|---|---|---|---|---|
| Pure rubber | 0 | 1.5677 | 1.6039 | 0.0362 | 1.0235 |
| Isotropic MREs | 10 | 3.6120 | 4.2267 | 0.6147 | 1.1614 |
| | 20 | 4.1569 | 5.2435 | 1.0866 | 1.2511 |
| | 30 | 5.4031 | 6.5846 | 1.1815 | 1.2133 |
| Anisotropic MREs (∥) | 10 | 2.5605 | 3.3381 | 0.7776 | 1.3037 |
| | 20 | 4.1864 | 5.8756 | 1.6892 | 1.4035 |
| | 30 | 6.6222 | 11.5133 | 4.8911 | 1.7386 |
| Anisotropic MREs (⊥) | 10 | 2.4732 | 3.3324 | 0.8592 | 1.3526 |
| | 20 | 4.2857 | 6.5274 | 2.2390 | 1.4620 |
| | 30 | 6.6266 | 8.2615 | 1.6349 | 1.2689 |

alignment was oriented along the same direction as the magnetic field of 67.5 mT. To put these results into perspective, previous tests reported by the authors on the same material under uniaxial compression revealed a 111% MR increase under the influence of a magnetic field of 450 mT, and even higher increases of 284% in uniaxial tensile tests were measured when the MRE was under the influence of a magnetic field of 289 mT. In both tests samples were strained up to 50% [16]. The equi-biaxial tension tests are an important part of a comprehensive dataset [16] and are required in order to fully characterize the complex behaviour of MREs to facilitate the future development and evaluation of accurate constitutive models [10]. However, several improvements to the test procedure reported in this paper can be suggested for future implementation:

(i) Perhaps the most important point is to improve measurement of either the horizontal force or the moment at the test machine (in addition to the measured vertical force). This would make all the assumptions described in section 6 redundant and any errors associated with these assumptions would then be eliminated. Redesigning the rig to include biaxial or torque load-cells would improve the quality of the results obtained from the equi-biaxial tension tests.

(ii) Improvement of the clamping system, and a larger stiffness of the sliding clamps (see section 3) to enable testing of the MRE samples up to larger strains.

## Acknowledgments

## References

[1] Jolly M, Carlson J, Munoz B and Bullions T 1996 The magnetoviscoelastic response of elastomer composites consisting of ferrous particles embedded in a polymer matrix *J. Intell. Mater. Syst. Struct.* **7** 613–22

[2] Lokander M 2004 Performance of magnetorheological rubber materials *PhD Thesis* Department of Fibre and Polymer Technology, Royal Institute of Technology, Stockholm

[3] Albanese Lerner A 2005 The design and implementation of a magnetorheological silicone composite state-switched absorber *Master's Thesis* School of Mechanical Engineering, Georgia Institute of Technology

[4] Gong X, Liao G and Xuan S 2012 Full-field deformation of magnetorheological elastomer under uniform magnetic field *Appl. Phys. Lett.* **100** 211909

[5] Bica I 2011 Magnetoresistor sensor with magnetorheological elastomers *J. Indust. Eng. Chem.* **17** 83–9

[6] Varga Z, Filipcsei G and Zrinyi M 2006 Magnetic field sensitive functional elastomers with tuneable elastic modulus *Polymer* **47** 227–33

[7] Stepanov G, Abramchuk S, Grishin D, Nikitin L, Kramarenko E and Khokhlov A 2007 Effect of a homogeneous magnetic field on the viscoelastic behavior of magnetic elastomers *Polymer* **48** 488–95

[8] Farshad M and Le Roux M 2005 Compression properties of magnetostrictive polymer composite gels *Polym. Test.* **24** 163–8

[9] Gudmundsson I 2011 A feasibility study of magnetorheological elastomers for a potential application in prosthetic devices *Master's Thesis* Faculty of Industrial Engineering, Mechanical Engineering and Computer Science, School of Engineering and Natural Sciences, University of Iceland

[10] Ogden R, Saccomandi G and Sgura I 2004 Fitting hyperelastic models to experimental data *Comput. Mech.* **34** 484–502

[11] BS 903-5 2004 Physical Testing of Rubber: V. Guide to the Application of Rubber Testing to Finite Element Analysis

[12] Ogden R W 1972 *Proc. R. Soc.* A **326** 565–84

[13] Merodio J and Ogden R 2005 *Int. J. Non-Linear Mech.* **40** 213–27

[14] Bustamante R 2010 *Acta Mech.* **210** 183–214

[15] Zhou Y, Jerrams S, Betts A and Chen L 2013 The effect of microstructure on the dynamic equi-biaxial fatigue behaviour of magnetorheological elastomers *8th European Conf. on Constitutive Models for Rubbers* (*ECCMR VIII*)

[16] Schubert G and Harrison P 2015 *Polym. Test.* **42** 122–34

[17] Schubert G and Harrison P 2015 *J. Magn. Magn. Mater.* submitted

[18] Schubert G, Harrison P and Guo Z 2013 The behaviour of magneto-rheological elastomers under equi-biaxial tension *19th Int. Conf. on Composite Materials* (*Montreal*)

[19] Comsol 2011 Comsol Multiphysics 4.2 Documentation ©1998-2011 COMSOL (http://comsol.com/comsol-multiphysics)

[20] Guo Z, Shi X, Peng X, Harrison P, Gosling P and Ogden R 2014 *Mech. Mater.* **70** 1–7